THE JOURNAL OF PHYSICAL CHEMISTRY B

Article

pubs.acs.org/JPCB

Observed Mechanism for the Breakup of Small Bundles of Cellulose Iα and Iβ in Ionic Liquids from Molecular Dynamics Simulations

Brooks D. Rabideau,* Animesh Agarwal, and Ahmed E. Ismail*

Aachener Verfahrenstechnik: Molecular Simulations and Transformations, Faculty of Mechanical Engineering, RWTH Aachen University, Schinkelstraße 2, 52062 Aachen, Germany

Supporting Information

ABSTRACT: Explicit, all-atom molecular dynamics simulations are used to study the breakup of small bundles of cellulose Iα and Iβ in the ionic liquids [BMIM]Cl, [EMIM]Ac, and [DMIM]DMP. In all cases, significant breakup of the bundles is observed with the initial breakup following a common underlying mechanism. Anions bind strongly to the hydroxyl groups of the exterior strands of the bundle, forming negatively charged complexes. Binding also weakens the intrastrand hydrogen bonds present in the cellulose strands, providing greater strand flexibility. Cations then intercalate between the individual strands, likely due to charge imbalances, providing the bulk to push the individual moieties apart and initiating the separation. The peeling of an individual strand from the main bundle is observed in [EMIM]Ac with an analysis of its hydrogen bonds with other strands showing that the chain detaches glucan by glucan from the main bundle in discrete, rapid events. Further analysis shows that the intrastrand hydrogen bonds of each glucan tend to break for a sustained period of time before the interstrand hydrogen bonds break and strand detachment occurs. Examination of similar nonpeeling strands shows that, without this intrastrand hydrogen bond breakage, the structural rigidity of the individual unit can hinder its peeling despite interstrand hydrogen bond breakage.

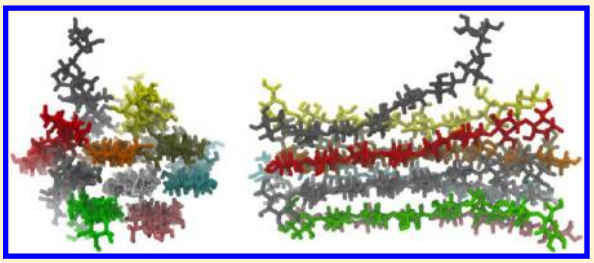

INTRODUCTION

The conversion of waste biomass into clean, sustainable biofuels has the potential to significantly aid in meeting the world's future energy demands while mitigating the environmental impact associated with energy production and use.[1] In the past ten years, a number of ionic liquids (ILs) have been shown to effectively dissolve cellulose.[2−6] Further, since many of these ILs have extraordinarily low volatility,[7] their choice as a solvent could guard against their unintentional release into the environment, offering an improved alternative over most traditional solvents.

Though a number of effective cation−anion combinations have been identified,[8] the sheer numbers of ionic species leads to an astronomical combination of possible pairs,[9] which, along with the diversity of ionic species involved, makes it conceivable that other combinations exist with even more desirable properties. Experimental testing of even a small fraction of all of these possibilities is not feasible and future success must rely on smarter screenings directed by fast computational methods[10] or by a fundamental understanding of the IL behavior. Past success has primarily come from exploring similar classes of cations, such as imidazolium-based and pyridinium-based molecules as well as good hydrogen-bond-accepting anions, such as chloride, acetate, and dimethyl phosphate.

Generally, it is believed that an IL's ability to dissolve cellulose rests strongly upon the hydrogen-bond accepting ability of the anion. Less clear, however, is the exact role the cation plays in dissolution.[8] Interestingly, some of the good hydrogen-bond-accepting anions that have been found to dissolve cellulose can be rendered ineffective through pairing with certain cations. For example, the imidazolium-based chlorides show an odd−even effect at short chain lengths,[4,11] while the pairing of the usually effective acetate anion with N-methyl piperdinium has been shown to hinder acetate's ability to dissolve cellulose.[12] Recently, the role of the cation in cellulose dissolution has been debated, with NMR studies of [BMIM]Cl suggesting that the cation formed hydrogen bonds with cellulose.[13,14] Others, however, have voiced their skepticism of this interpretation.[15,16]

Molecular dynamics (MD) simulations have proven valuable to better understand how cellulose interacts with ILs. Studies looking at the interactions of [DMIM]Cl with glucose[17] and [EMIM]Ac with individual cellulose strands[18] have shown the strong interactions occurring between the anions and the hydroxyl groups of cellulose. Later studies have examined conformational changes of cellulose Iβ in [EMIM]Ac[19] and looked at the antisolvent behavior of water.[20] Other studies looking at the interaction of [BMIM]Cl with crystalline cellulose have highlighted the dominant role of intersheet interactions,[21] the importance of solvent versatility in disrupting these interactions,[22,23] and the role that solvent entropy plays in

Received: October 16, 2012
Revised: March 7, 2013
Published: March 9, 2013

cellulose dissolution.[24] Other studies examining the recalcitrance of crystalline cellulose during enzymatic hydrolysis calculated decrystallization free energies for various surface strands[25,26] finding different energies associated with different lattice positions.

Even so, there still remains a significant gap in our understanding of the dissolution of cellulose by ILs. Notably, there is no clear understanding of the role of individual ionic species in dissolution. Others have hypothesized that in some cases anions might bind to cellulose and these polyanionic moieties are then separated by the cations,[8,17] although little concrete evidence supports this view. Further, most past theoretical studies have focused on single cation−anion combinations, making generalizations about each species' role difficult. A deeper understanding of the precise roles of individual ionic species could significantly enhance our understanding of cellulose dissolution, possibly leading to new cation−anion combinations and improved solvent effectiveness for processes focusing on the breakup and separation of cellulose from its native state.

In this paper, we present explicit all-atom MD simulations showing the breakup of small bundles of crystalline cellulose in the ILs 1-butyl-3-methylimidazolium chloride ([BMIM]Cl), 1-ethyl-3-methylimidazolium acetate ([EMIM]Ac), and 1,3-dimethylimidazolium dimethylphosphate ([DMIM]DMP). These ILs are known to be highly effective in dissolving cellulose, are widely available commercially, and have sufficient diversity in their ionic species to offer a perspective on the role of the cations and the anions. In all cases, we find a common mechanism leading to the breakup of individual strands. Anions bind strongly to the exterior hydroxyl groups of the individual cellulose strands weakening the intrastrand hydrogen bonds and disrupting the rigidity of the individual cellulose strands. The bound anions cause cellulose to behave effectively as a negatively charged complex, while the cations slip between individual strands. This cation movement is likely due to resultant charge imbalances; the presence of the cations between strands provides the bulk needed to push these complexes apart.

In the next section, our simulation protocols are presented, including the force fields and cellulose morphologies used. This is then followed by the results of individual cellulose strands with the ILs, yielding insight into their fundamental interactions. Next, results for the small cellulose bundles are presented. First, the stability of the Iα and Iβ bundles is probed in aqueous simulations to ensure there is no significant instability in the models. Then, the dissolution of Iα and Iβ bundles in the different ILs is presented along with a detailed analysis of the underlying behavior. Next, the peeling behavior of one of the strands in both the Iα and Iβ morphologies is examined in detail, providing further insight into the underlying mechanisms. Finally, a summary of the main results is given along with the general conclusions of this study.

SIMULATION METHODS

Modeling. Cellulose (shown in Figure 1) was modeled with the OPLS-2005 force-field.[27,28] Crystalline bundles of cellulose Iα and cellulose Iβ were constructed from crystallographic data obtained through X-ray and neutron scattering experiments.[29,30] The imidazolium-based cations [BMIM], [EMIM], and [DMIM] (shown in Figure 2) as well as the chloride anion were modeled using the general force field developed by Canongia Lopes et al.[31] This model has been

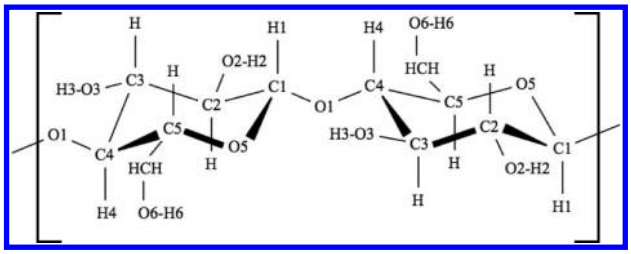

Figure 1. Structure of the repeat unit of cellulose.

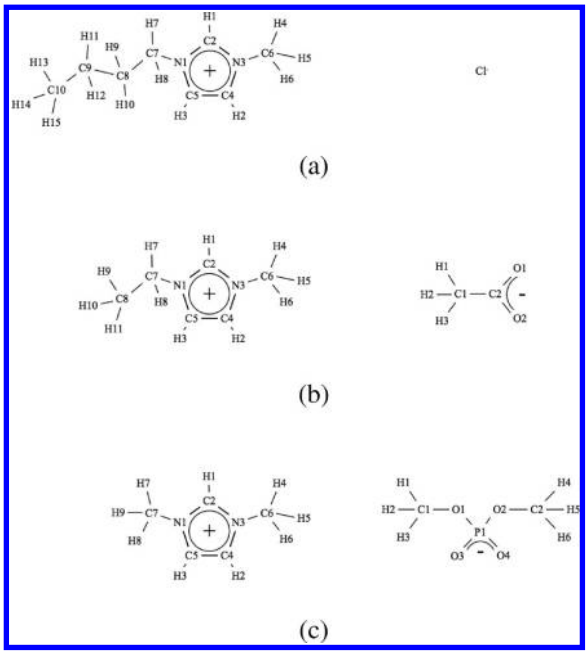

Figure 2. Chemical structures of (a) [BMIM]Cl, (b) [EMIM]Ac, and (c)[DMIM]DMP.

employed extensively, was constructed to allow consistent pairing of different cation and anion combinations, and was validated against available solid and liquid state properties. Importantly, it is also based upon the OPLS framework, making it compatible with the other force fields employed in this study. As specified by the force field, all C−H bonds of the cations were constrained using the SHAKE algorithm.[32] The remaining acetate (Ac) and dimethylphosphate (DMP) anions were modeled using OPLS-AA.[27] To ensure that the cellulose models were not inherently instable, aqueous simulations were performed using the SPC/E force field[33] in conjunction with the SHAKE algorithm. All simulations in this study were carried out with the LAMMPS MD package.[34]

Cellulose Morphology. Three distinct morphologies are examined in this study: a single strand, consisting of 16 glucose units, and Iα and Iβ crystalline bundles, consisting of eight glucose units per strand. While we are mainly interested in crystalline bundles, their structural complexity makes isolating their fundamental interactions with ILs difficult. For this reason, individual strands were also studied, as the elimination of other chains yields insight into the interactions of individual glucan units with the ILs. To ensure that the properties presented herein correspond to a near-equilibrium state, simulations were carried out using an elongated strand as the initial configuration. The atomic positions of this strand are determined from crystallographic data.[29,30]

dx.doi.org/10.1021/jp310225t | J. Phys. Chem. B 2013, 117, 3469−3479

For the simulations involving cellulose bundles, a small cellulose Iα bundle consisting of six strands each with eight glucose units (Figure 3b) and a larger cellulose Iβ bundle

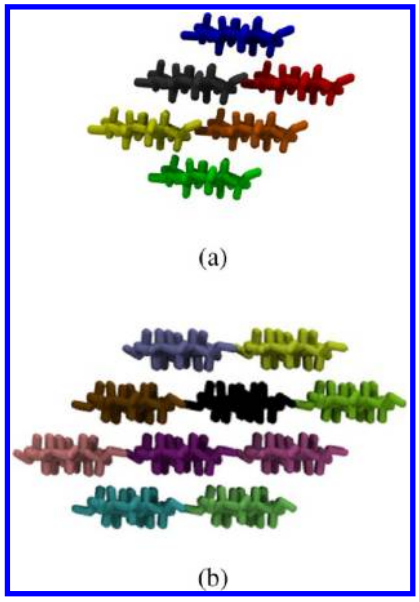

Figure 3. Small crystalline bundle of (top) cellulose Iα and (bottom) cellulose Iβ examined in this study.

consisting of ten strands each with eight glucose units (Figure 3a) were constructed. It is worth noting that the intention here is not for a direct comparison of the different cellulose structures, since they are noticeably different, but rather to test two bundles with varying structural integrity. Figure 3 illustrates that the Iα bundle is rather weakly bound with no internal strands while the Iβ bundle is slightly more robust, having two internal cellulose strands. It should be kept in mind that the bundles examined in this study are noticeably smaller than some natural cellulose fibers that have been successfully characterized.[35] Because of the computational cost of studying realistic cellulose fibers, the aim of this study focuses on understanding the role of ionic species in separating initially ordered cellulose strands of varying integrity.

Simulation Details. Before beginning the simulations with cellulose, separate simulations are carried out to ensure equilibration of the solvents. Starting configurations are constructed using Packmol,[36] with initial densities equal to experimental values at the respective temperatures and pressures. Cubic simulation boxes are constructed with lengths of approximately 60 Å and typically contained about 30 000 atoms. Larger boxes are required to accommodate the 16-glucan single strand of straightened cellulose; for these simulations, the *z*-axis is extended to 100 Å. In all cases, a cutoff of 12 Å is used and long-range electrostatics computed with the particle−particle particle−mesh (PPPM) method developed by Edwards and Hockney.[37] These starting structures are then equilibrated in an *NPT* ensemble for 3 ns. IL simulations are conducted at 400 K and aqueous simulations at 298 K, each connected to a Nosé-Hoover thermostat with a thermocouple of 100 fs. All solvents are simulated using a Nosé-Hoover barostat, at a pressure of 1 bar with a barocouple of 1000 fs.[38]

After equilibrating the solvents, the corresponding cellulose strand or bundle is placed within the simulation box. Any cation or anion atom within 2 Å of any cellulose atom leads to the removal of that respective ion. Surplus ions are then removed according to their proximity to the introduced cellulose to ensure charge neutrality. The combined cellulose−solvent system then undergoes a series of six 10-fold increases in the time step size, each for 1000 timesteps, until 1 fs is reached. The simulation continues for 3 ns in an *NPT* ensemble before switching to an *NVT* ensemble for the remaining time. All atom positions are output every 20 000 timesteps, while those of cellulose are ouput every 500 timesteps.

RESULTS AND DISCUSSION

Behavior of Individual Strands. To observe the direct interactions of the solvents with cellulose, we have simulated an individual strand of sixteen glucose units in each of the solvents. When dealing with long flexible strands, it is helpful to measure properties at a near equilibrium state. This can be rather difficult since ILs, under certain circumstances, have been shown to bind multiple hydroxyl groups together, inhibiting evolution toward an equilibrium state.[39]

One way to gauge a strand's evolution is to measure its radius of gyration, defined as

$$R_g^2 = \frac{1}{M}\sum_i m_i|\mathbf{r}_i - \mathbf{r}_{cm}|^2 \quad (1)$$

in which M is the total mass, m_i and $\mathbf{r}_i$ are the mass and position of atom i, and $\mathbf{r}_{cm}$ is the position of the center of mass. An analysis of the evolution of the elongated states should indicate how far each strand is from a near-equilibrium state. The evolution of the radius of gyration for each IL is given in Figure 4. As the simulations proceed, the initially elongated strands show little variation in the radius of gyration, indicating that they are already near equilibrium.

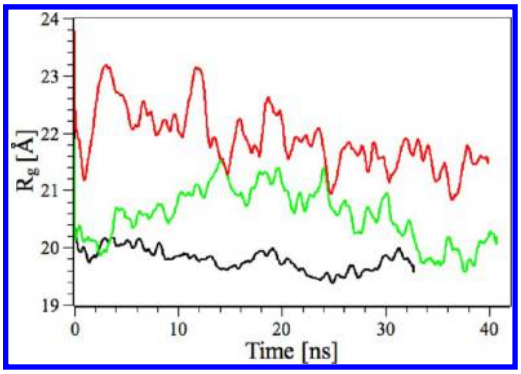

Figure 4. Radius of gyration as a function of time for the single-stranded, 16 glucose-unit cellulose in [BMIM]Cl (black), [EMIM]Ac (red), and [DMIM]DMP (green).

Cylindrical distribution functions (CDF) can reveal patterns in the charge distribution away from the long axis of the strand. A typical CDF for [EMIM]Ac is shown in Figure 5 while the others are given in the Supporting Information. The cylindrical charge distribution oscillates, going from positive to negative and again positive at 3 Å, 4 Å, and 5 Å. This oscillation continues to approximately 20 Å in all three ILs. In each case, the cations are found closest to the glucose unit. This was previously observed for [BMIM]Cl[23] and attributed to increased contacts along the axial directions of the glucose-units, the direction responsible for intersheet contacts. Specific

dx.doi.org/10.1021/jp310225t | J. Phys. Chem. B 2013, 117, 3469−3479

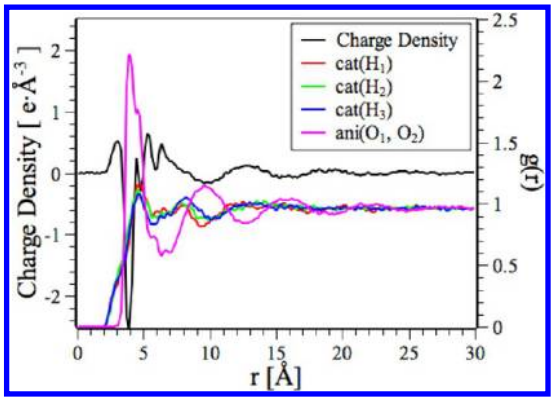

Figure 5. Cylindrical distribution function showing charge distribution and the radial distribution function for [EMIM]Ac in the single strand simulation. Abbreviations refer to (cel) cellulose, (cat) cation, and (ani) anion. Labeled atoms refer to Figure 1 and Figure 2.

interactions can be probed further by constructing site−site distribution functions between similar categories of atoms in the IL and cellulose. These functions are given in Figure 6.

In [EMIM]Ac and [DMIM]DMP (Figure 6b,c) the dominant contribution to the structure is the association of the resonant oxygens of the anions with the hydroxyl groups of cellulose. Another smaller, yet significant, contribution comes from these same resonant oxygens with the C_1 and C_4 hydrogens of cellulose, corresponding to the large anion density seen in the spatial distribution functions. Further, Figure 6c shows that the P−O−CH_3 oxygens of DMP play a very minor role. Similarly, in [BMIM]Cl (Figure 6a), the interactions of chloride with the hydroxyl groups of cellulose also dominate. However, the chloride ion's interaction with the C_1 and C_4 hydrogens of cellulose appears to be less than that of the other ILs. Importantly, there is little contribution from the cations in any IL. A more thorough examination of hydrogen bonding between each cation and cellulose was performed using a set of geometric criteria:[40−45] the distance between the hydrogen to the accepting nitrogen must be less than 2.45 Å, the distance between the two oxygen atoms must be less than 3.5 Å, and the nitrogen acceptor—oxygen donor—hydrogen angle must be less than 30°. Using these criteria, no convincing evidence of significant hydrogen bonding between the cation and cellulose was found.

Extending the hydrogen-bond analysis to the anionic interactions with the different hydroxyl and methylhydroxyl groups of cellulose yields the averages for each hydroxyl unit determined on a per glucan basis as summarized in Table 1. The ratio of anions to hydroxyl groups ranges from approximately 0.8 for DMP to nearly 0.92 for acetate. In all cases, the methylhydroxyl group (H_6) contributes slightly less than each of the neighboring hydroxyl groups (H_2 and H_3).

Table 1. Average Number of Hydrogen Bonds per Hydroxyl Group in the Three ILs

IL	H_2	H_3	H_6	Total
[BMIM]Cl	0.82	0.84	0.78	2.48
[EMIM]Ac	0.94	0.93	0.87	2.75
[DMIM]DMP	0.79	0.87	0.76	2.39

A further breakdown of the individual contributions to the hydrogen bonds is given in Table 2. Here, the diagonal elements represent individual hydrogen bonds with the respective atom, while the off-diagonal elements refer to bridging hydrogen bonds between the hydrogen atoms of the respective row and column. Comparing Ac and DMP, it is seen that the individual hydrogen bond contributions are quite similar, while the major reduction in overall hydrogen bonding in DMP comes from a reduction in bridging interactions. It is quite possible that DMP's larger size and ensuing rotational freedom contribute to this reduction while the much smaller Ac ion is more agile and can maneuver toward these energetically favorable positions. As mentioned earlier, it is generally agreed

Table 2. Average Number of H-Bonds per Glucose Unit for the ILs[a]

IL		H_2	H_3	H_6	Total
[BMIM]Cl	H_2	0.32	0.35	0.19	0.87
	H_3	0.35	0.27	0.18	0.81
	H_6	0.19	0.18	0.42	0.79
[EMIM]Ac	H_2	0.24	0.59	0.19	1.02
	H_3	0.59	0.31	0.09	1.00
	H_6	0.19	0.09	0.63	0.92
[DMIM]DMP	H_2	0.27	0.42	0.11	0.80
	H_3	0.42	0.35	0.12	0.89
	H_6	0.11	0.12	0.55	0.79

[a]Diagonal elements H_i−H_i represent individual H-bonds with the respective atom; off-diagonal elements H_i−H_j refer to bridging H-Bond between the respective atoms and includes bridges within the same glucose unit and between different glucose units. Standard deviations are presented in the Supporting Information.

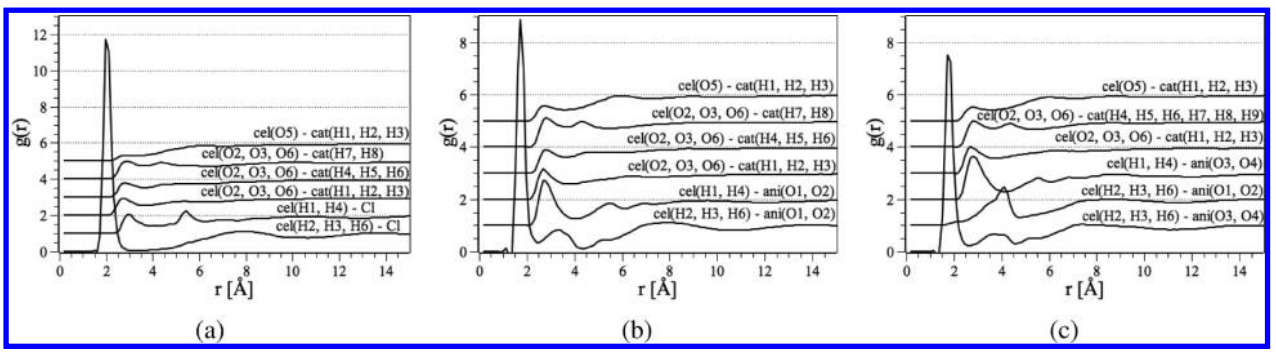

Figure 6. Selected partial radial distribution functions between glucose units, anions, and cations for (a) [BMIM]Cl, (b)[EMIM]Ac, and (c)[DMIM]DMP. Averages are taken over all the 16 glucose units. Interactions between glucose oxygens and IL cation hydrogens are presented as averages over all similar centers. Abbreviations refer to (cel) cellulose, (cat) cation, and (ani) anion. Labeled atoms refer to Figure 1 and Figure 2.

dx.doi.org/10.1021/jp310225t | J. Phys. Chem. B 2013, 117, 3469−3479

that the hydrogen-bond accepting ability of the anion plays a large role in the dissolution of cellulose, and the differences seen here could play a role in the observed dissolution rates as well as the overall solubility.

Stability of Bundles in Water. It is well-known that cellulose Iα and Iβ are thermodynamically stable in water and experience a certain resistance to enzymatic hydrolysis.[46] In fact, water seems to have an antisolvent property with cellulose when in the presence of typically dissolving ILs.[2,20] To ensure that there are no major, inherent instabilities in the simulation of the cellulose bundles, we studied the behvior of Iα and Iβ bundles in water. Because of the computational investment required to carry these simulations out to the microsecond time scale, as has been done for other models,[47] we only examine times that are comparable with the IL simulations of the later sections. Following the standard preparation of the simulation, cellulose Iα and Iβ bundles were simulated in SPC/E water at 298 K and 1 bar for 60 ns. It must be stressed that the validity of this stability holds only for the time scales examined in this study.

During simulation, the structures undergo a fair amount of motion, including significant rotation and even a small torsion that has previously been explored.[48] Some strand ends even peel momentarily from the main bundle only to reform nanoseconds later. However, the underlying positional arrangement remains intact during this time as shown by the final structures given in Figure 7.

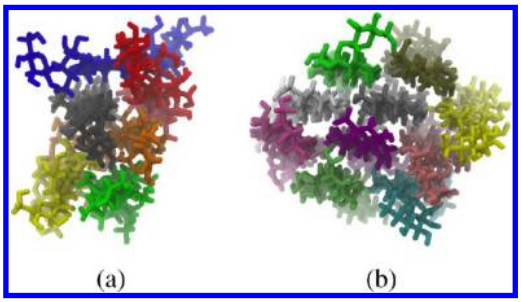

Figure 7. Aqueous simulations of the (a) cellulose Iα bundle and (b) cellulose Iβ bundle after 60 ns of simulation.

This stability can be quantified by calculating the number of interstrand hydrogen bonds. These results show convergence toward a finite value in both cases, as shown in Figure 8. Though the number of interstrand hydrogen bonds in the case of Iα are significantly lower than expected, and there are slight

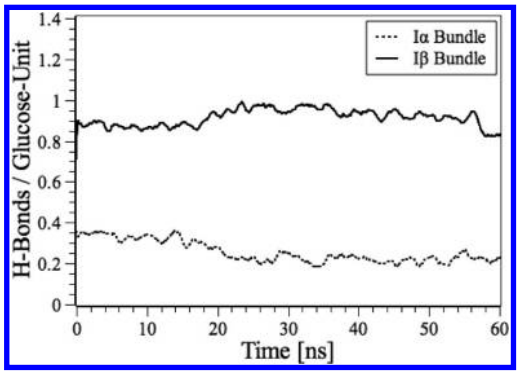

Figure 8. Evolution of the interstrand hydrogen bonds of the bundles in water.

changes in the crystalline structure, as seen in Figure 7a, an analysis of center-to-center glucose distances in the next section shows no significant separation of the strands during the simulation.

In the next few sections, we will observe spontaneous dissociation of cellulose bundles in ILs. We note here that the water simulations do not show significant instability in the bundles and appear resistant to breakup during the observed timespans.

Dissolution of Iα Bundles in ILs. Cellulose Iα bundles were simulated in each IL for a minimum of 75 ns. Each IL showed a significant breakup of the main bundle compared to water. Of the three ILs, [EMIM]Ac clearly produced the most rapid breakup of individual strands, which resulted in the greatest bundle decomposition. The final structure is given in Figure 9a. After 86 ns, the structure has clearly lost its crystalline structure, now resembling just a loosely connected mass of well-dispersed strands. During this process both ends of the bundle exhibit fraying, which propagates toward the center of the bundle.

A closer look at the underlying cause of the initial strand separation reveals that acetate anions form hydrogen bonds with the hydroxyl groups of cellulose, oriented along the equatorial plane of the glucan units. Meanwhile, the cations associate with these anions and, in doing so, force themselves between the separating strand and the main bundle. This initial deformation and the ensuing separation can be attributed to the bulk of the cation. This configuration of cations and anions is illustrated in Figure 9b. Further, the formation of hydrogen bonds with acetate is at the expense of the intrastrand hydrogen bonds, weakening the structure and increasing the flexibility of the separating strand. In turn, this facilitates penetration of more cations into the bundle interior.

Examining the individual contributions to the potential energy experienced by an individual strand during dissolution further elucidates this process (see Figure 10). Large separation events are characterized by jumps in the potential energy contributions. During these jumps there is a favorable energy contribution from the anions (negative values) and an unfavorable contribution from the cations (positive values). This implies that, during these initial jumps, the cations associate with the bound anions at the expense of their positions with respect to cellulose. Soon thereafter, the system relaxes and both cations and anions provide favorable contributions to the strand.

This same mechanism is also seen for [BMIM]Cl and [DMIM]DMP, though these breakups occur at slower rates. The reduction in overall hydrogen bond formation that was observed for DMP in the single strand case, which was attributed to the larger size and hindered rotation, likely affects [DMIM]DMP's overall breakup rate. Experimentally, [BMIM]-Cl has the highest viscosity of the three ILs, as was readily apparent from the simulations. Specifically, the binding of chloride ions to the hydroxyl groups of cellulose tends to pin cellulose's movement, reducing the overall dissolution rate. [BMIM]Cl showed the slowest rate of breakup, yet there was an unobstructed view of the initial strand separation. As with the other ILs, the anions bind tightly to the hydroxyl groups of cellulose where they linger for the duration of the simulation.

As the cellulose strands begin to separate from the main bundle there are, surprisingly, no chlorides present between the separating strand and the main bundle. A closer look reveals only cations in this interior space, providing the bulk needed to

dx.doi.org/10.1021/jp310225t | J. Phys. Chem. B 2013, 117, 3469−3479

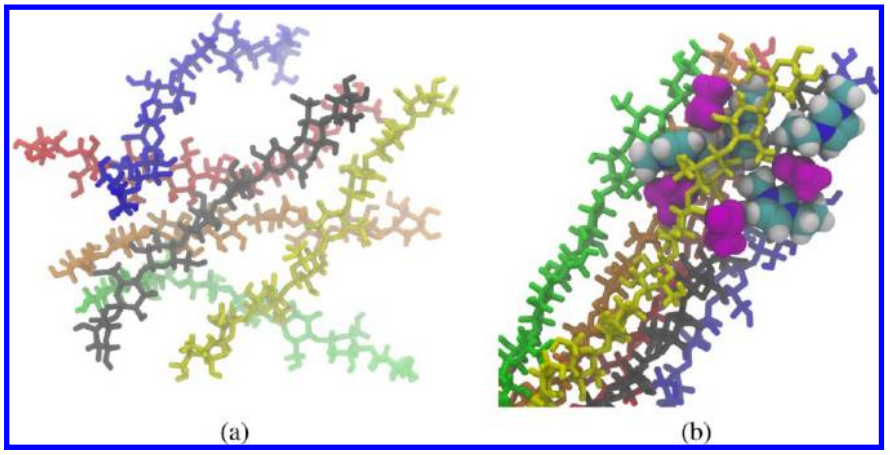

Figure 9. Structure of a cellulose Iα bundle in [EMIM]Ac (a) after 86 ns and (b) at approximately 1 ns showing the initial separation of an individual strand (yellow) from the cellulose Iα bundle in [EMIM]Ac. The anions (magenta) bind with the hydroxyl groups of cellulose, while the cations (cyan and white) force themselves between the separating strand and the main bundle.

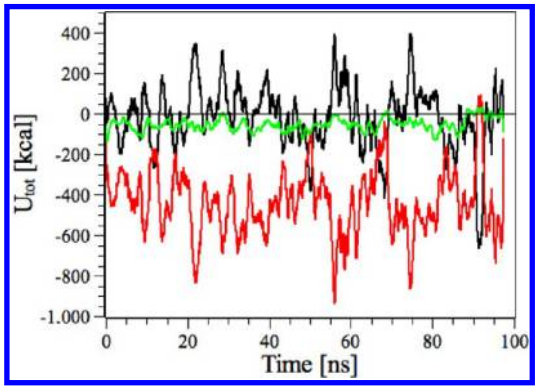

Figure 10. Pairwise energies experienced by one of the Iα strands in [EMIM]Ac attributed to (black) cations, (red) anions, and (green) other cellulose strands.

separate the strands. The participation of the large cations appears to be even more crucial in the case of [BMIM]Cl, because of the small size of Cl^- and its inability to provide significant separation. The initial stages of this deformation can be traced back to a single cation wedging itself at the midpoint of one of the exterior strands. This wedging creates a bow in the middle of the strand, which propagates outward as more cations enter this newly formed cavity. Once the propagation reaches the end of the strand, exactly half of the strand remains freely floating in the solvent. Various stages of this strand separation are shown in Figure 11. The observation of strand separation initiating from the midpoint of the bundle is potentially of great relevance, since real cellulose fibers are composed of many thousands of repeat units, making initiation at interior glucan units much more likely.

Together these simulations suggest a common mechanism for the initial breakup of cellulose fibers. Anions bind strongly with the hydroxyl groups of cellulose to form negatively charged moieties, which are then separated with the cations acting as the "bulk". The prerequisite of strong anion binding might explain why a number of imidazolium-based chlorides dissolve cellulose while the respective bromides do not.[4] The weaker interaction of bromide ions with hydroxyl groups may

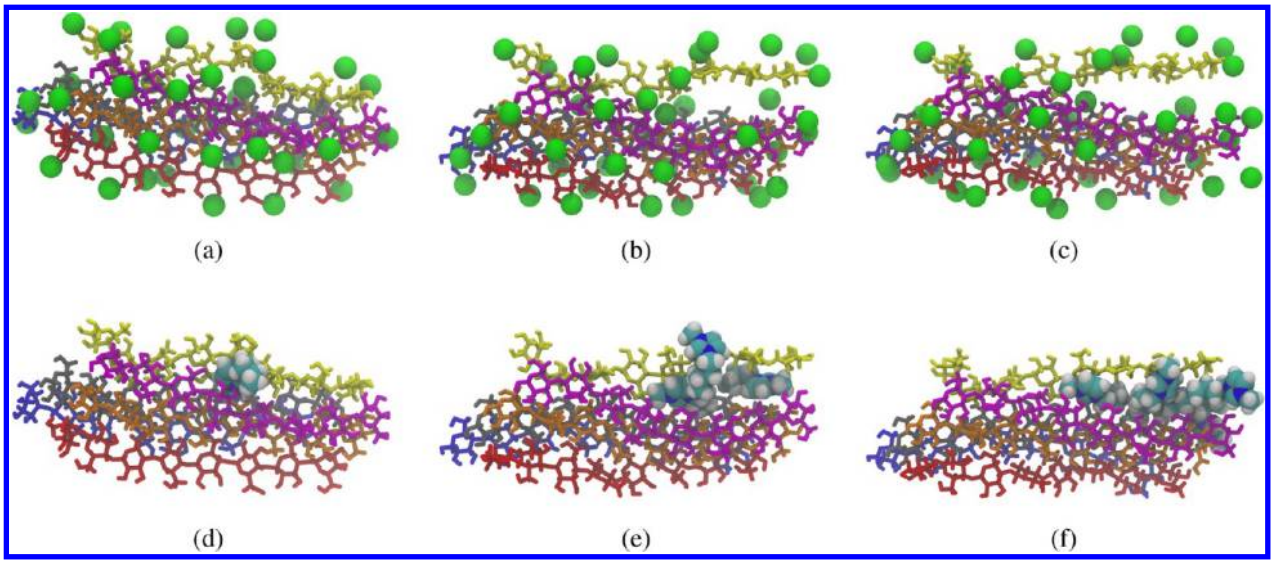

Figure 11. Cellulose Iα bundle in [BMIM]Cl showing contacting chlorides (top row, green) and penetrating cations (bottom row, cyan and white) after (a,d) 2 ns, (b,e) 50 ns, and (c,f) 55 ns.

dx.doi.org/10.1021/jp310225t | J. Phys. Chem. B 2013, 117, 3469−3479

preclude the formation of well-formed, negatively charged moieties.

To quantify the physical strand separation, nearest-neighbor distances are calculated based upon the centers of mass for each glucan unit, excluding same-strand distances. Units that have detached from the main bundle should be far removed from other centers of mass and thus have larger nearest-neighbor distances. These distances were calculated and averaged over all six strands for each of the eight individual glucan unit positions; the results are summarized in Figure 12.

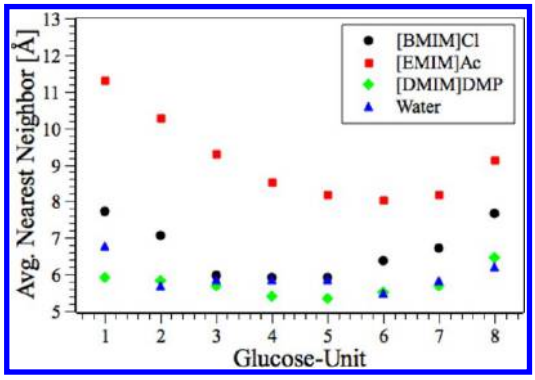

Figure 12. Average nearest-neighbor distance for each glucose unit, averaged over all strands, for the final states of the Iα simulations.

Dissolution of Iβ Bundles in ILs. The Iα bundles show a significant breakup in all three ILs, although their structure is also the weaker of the two studied, composed entirely of external strands. Unlike the Iα bundles, the Iβ bundles are slightly larger, including two internal strands, which allows us to gauge the effectiveness of these ILs in dissolving a more robust, and more realistic, cellulose fiber.

As expected, the Iβ bundles are much more resistant to breakup: however, sufficient strand detachment is observed to infer behavior. As before, the interaction with [BMIM]Cl seems to occur at a much slower rate when compared to the other ILs and the same mechanism is observed. Chlorides bind to the exterior hydroxyl groups of cellulose while the cations wedge themselves between strands, allowing them to separate.

In [DMIM]DMP, the Iβ bundle shows a large split occurring down the center plane of the bundle, as shown in Figure 13. The impetus for this split can be traced to an event at around 16 ns, when a single [DMIM] cation passes the large DMP anions sitting at the exterior of bundle and places itself between the top two cellulose strands (Figure 13b). This perturbation of the exterior bundle structure then allows more cations to enter the interior, propagating the initial split.

As with the Iα bundles, [EMIM]Ac shows the fastest dissolution rate of the three ILs and provides the most illustrative case of bundle breakup. The Iβ bundle in [EMIM]Ac shows an entire strand progressively detaching from the surface of the main bundle. Various stages of this process are shown in Figure 14, providing a look at the dynamics of individual strand peeling. Initially, one end of the dark gray strand detaches from the bundle, starting after just a few nanoseconds. This peeling continues unit by unit in sudden, discrete detachment events. Interestingly, these detachments occur axially, the direction responsible for intersheet contacts. As seen in the figure, the unbound portion of the strand appears to lose its rigidity and linearity, suggesting the loss of many of its intramolecular hydrogen bonds. Toward the end of

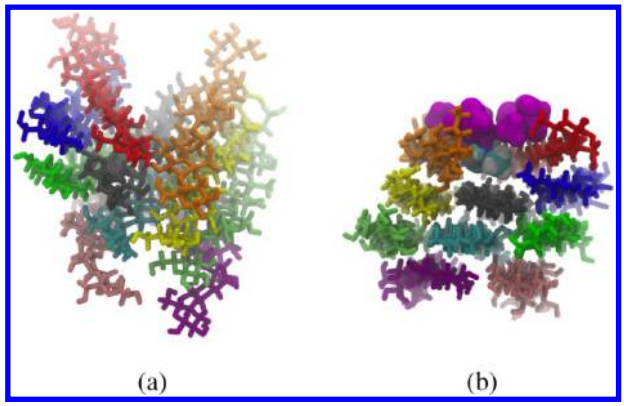

Figure 13. Structures of cellulose Iβ in [DMIM]DMP (a) after 80 ns showing a split occurring down the central axis and (b) the initiation of this split at 16 ns caused by the intercalation of a single cation (cyan and white) while the anions (magenta) remain exterior and hydrogen bonded to the cellulose bundle. Note that the two figures are shown from opposite ends of the bundle.

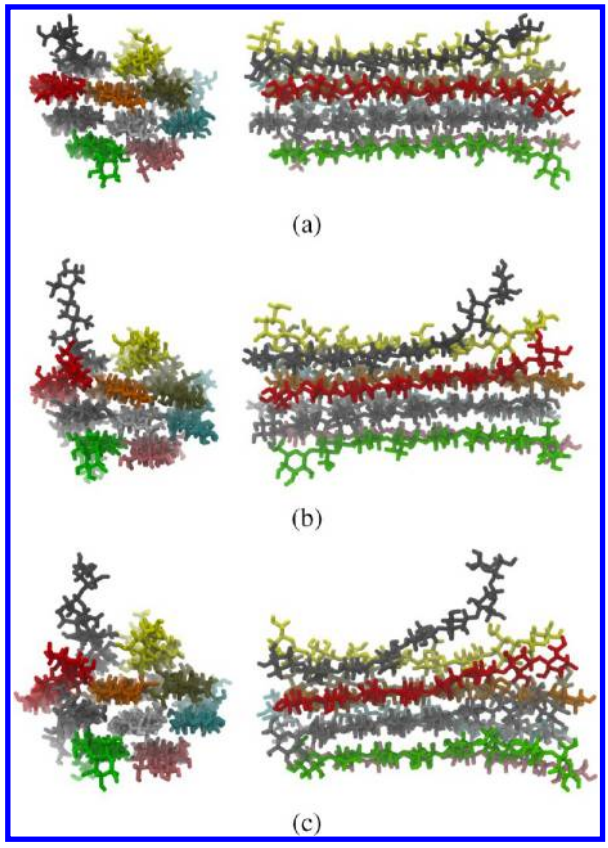

Figure 14. Evolution of cellulose Iβ in [EMIM]Ac showing the unzipping of a single strand (dark gray) after (a) 2 ns, (b) 6 ns, and (c) 14 ns.

the simulation, the strand remains attached at just one or two glucose units, and the neighboring yellow strand has already begun detaching from the opposite end. Interestingly, the dark gray strand occupies a corner lattice position in the Iβ bundle, a position previously shown as one of the easiest to remove in aqueous simulations based upon free-energy arguments.[25]

Interestingly, the dark gray strand of Figure 14 peels while the strand occupying the opposite corner, the pink strand, does not. While the two strands are similar, they are not identical. For clarity, we call the pink strand the mirror-image strand. The

dx.doi.org/10.1021/jp310225t | J. Phys. Chem. B 2013, 117, 3469−3479

difference in the individual contributions to the potential energy experienced by these two strands sheds light on why the former peels while the latter does not (see Figure 15). For the

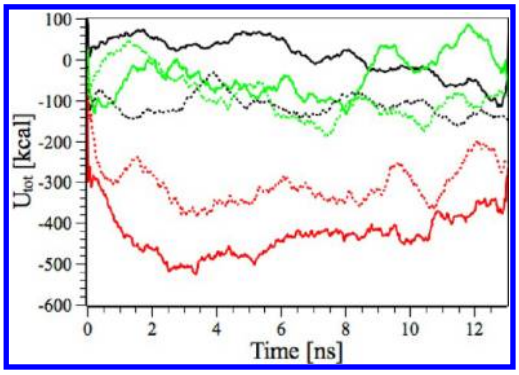

Figure 15. Pairwise energies experienced by (solid lines) the peeling strands and (dashed lines) the nonpeeling, mirror-image strand of the Iβ bundles in [EMIM]Ac. Colors indicate the contribution by (black) cations, (red) anions, and (green) other cellulose strands.

peeling strand, the anions (solid red lines) provide a considerably more favorable contribution when compared with those of the nonpeeling strand (dashed red lines). Importantly, the contributions from the cations in the peeling strand (solid black lines) remain positive and unfavorable with respect to the strand, while this is clearly not the case for the nonpeeling strand. This could indicate the importance of a critical number of anions at the exterior of the strand, which might precipitate the penetration of a cation into the cellulose bundle.

As with the Iα simulations, we can objectively quantify strand separation by calculating nearest-neighbor distances. Since the Iβ simulations show more localized separation, with the majority of the bundle remaining intact, an average would obscure these localized separations. Instead, the maximum value of all six strands is given for each of the eight glucan unit positions; the results are summarized in Figure 16. In

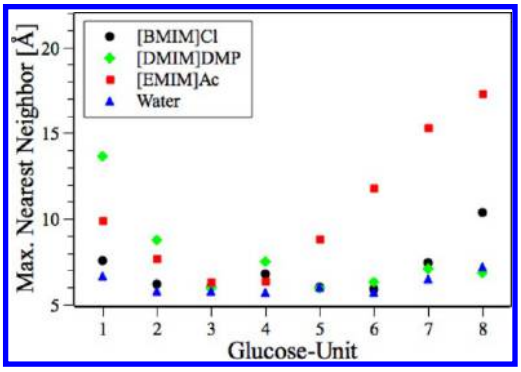

Figure 16. Maximum nearest-neighbor distance for each glucose unit in all strands, for the final states of the Iβ simulations.

comparing the results for Iβ and Iα (Figure 12) bundles, two differences become apparent. First, there is significantly less separation overall for Iβ, which is to be expected from a more robust crystalline network. The second main difference is that Iβ strands show significantly more strand separation in [DMIM]DMP compared to the Iα strands in [DMIM]DMP. The reason for this remains unclear, although DMP's reduced hydrogen bonding might require a greater cellulose surface area to induce a sufficient charge required to draw in cations to separate the strands.

Realistic Microfibers. As previously noted, the cellulose bundles examined in this study are significantly smaller than some natural cellulose fibers that have been successfully characterized.[35] To ensure that we can reproduce the behaviors found for small bundles in larger plant microfibers, we decided to test one such system. This realistic microfiber consisted of 36 cellulose strands, each with 60 glucose units in extent, arranged in a Iβ lattice that initially forms a flat square facet at both ends. Previously, an identical microfiber was tested using three different carbohydrate models in TIP3P water,[47] showing, among many other things, a relative stability for upward of 800 μs. As in the previous study, we modeled the microfibril using GLYCAM06,[49] which also allowed us to gauge the effect of using the OPLS-2005 carbohydrate force field to model cellulose. As this simulation was rather intensive, containing 129 069 atoms in a box of size 60 Å by 60 Å by 360 Å, it was possible to test only [EMIM]Ac. The initial and final structures of the microfiber are shown in Figure 17. After 80 ns of simulation we see a similar separation of individual strands from the main bundle. Not only did this occur for the topmost and bottommost strands in the lattice, but significant separation was also observed in neighboring strands. As before, the bundles showed a continued progression toward an unraveled state, which could be isolated to the same underlying mechanism seen for the smaller bundles. Though we only present results for [EMIM]Ac, these results suggest that the behavior of smaller systems can be relevant for much larger systems and that the choice of carbohydrate model, in this case, has little effect on the observed results.

Peeling of the Cellulose Chains. We now take a closer look at the peeling strand (dark gray in 14) of the Iβ bundle in [EMIM]Ac. The evolution of the interstrand hydrogen bonds with this strand is shown for individual glucan units in Figure 18. Peeling begins from the reducing end and each individual detachment occurs in a sudden, disjointed manner. The first and second units detach almost simultaneously around 2 ns followed by the third and fourth units at 10 and 12 ns (Figure 18b). Around 16 ns, the interstrand hydrogen bonds of the fifth unit break (green) while those of the next two units (light and dark blue) remain strong. Shortly thereafter the fifth unit reattaches.

A closer look at the evolution of all hydrogen bond types for the first four glucans (Figure 19) reveals that the intrastrand hydrogen bonds seem to affect the actual detachment of the individual units. The third and fourth units show that the intrastrand hydrogen bonds break for a sustained period of time before the interstrand hydrogen bonds break. Since these intrastrand hydrogen bonds contribute to the rigidity of the strand it seems sensible that a disruption of these bonds might be necessary for flexibility, facilitating the cations' entrance into the interior space and the subsequent pivoting of the glucose unit away from the main bundle.

If we look at the behavior of the strand opposite this peeling strand (the pink strand in Figure 14) the factors contributing to the stabilization of the end units become clearer. This strand occupies the opposite corner of the Iβ lattice, although it does not initiate peeling. The evolution of the hydrogen bonds for this strand is given in Figure 20. In this case the interstrand hydrogen bonds are quickly broken within a few nanoseconds, while the intrastrand hydrogen bonds remain strong for up to 15 ns. Though the interstrand hydrogen bonds remain

dx.doi.org/10.1021/jp310225t | J. Phys. Chem. B 2013, 117, 3469−3479

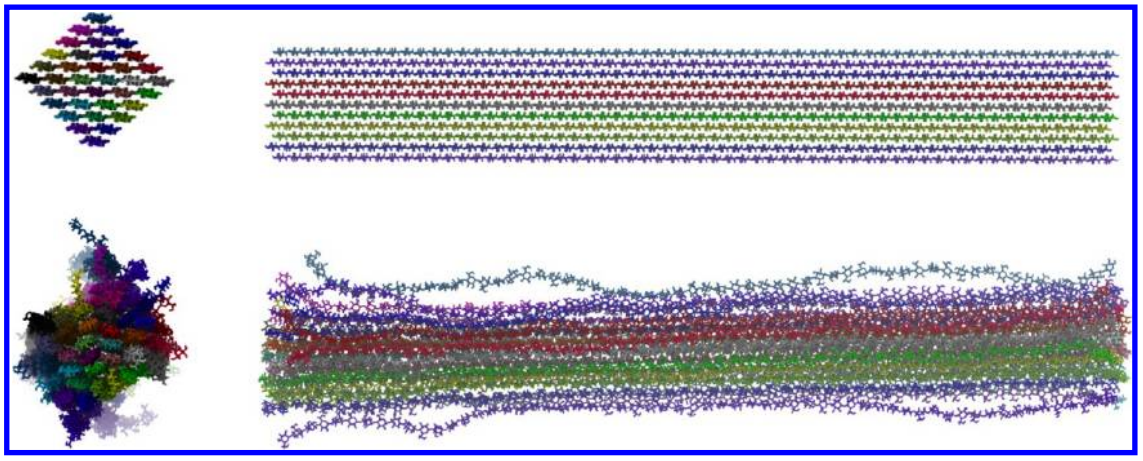

Figure 17. Large, realistic cellulose Iβ microfiber consisting of 36 strands, each 60 glucose units in extent (top) initially and (bottom) after 80 ns of simulation.

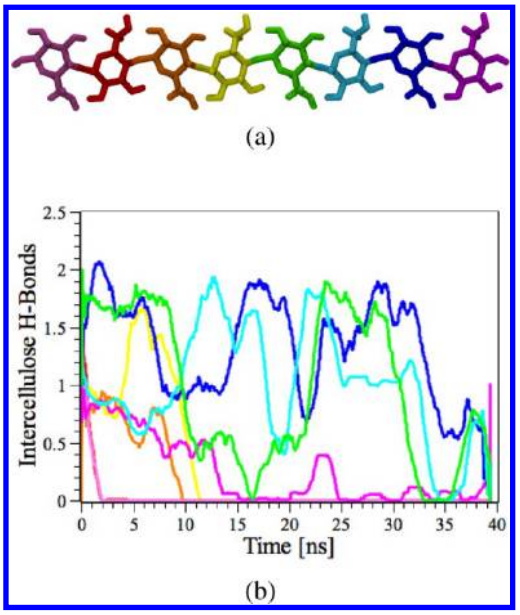

Figure 18. Evolution of interstrand hydrogen bonds in the peeling strand of Figure 14. The colored lines of (b) refer to the individual glucose units given in (a).

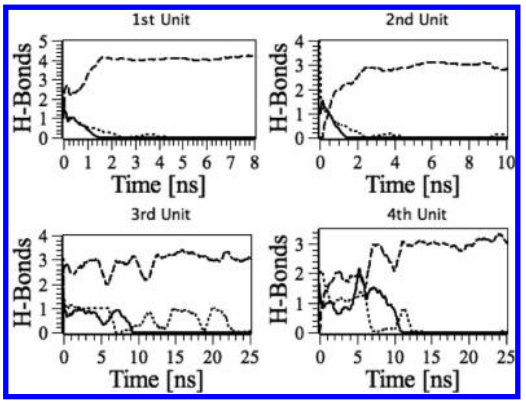

Figure 19. Evolution of intrastrand (dotted lines), interstrand (solid lines), and solvent-strand (dashed lines) hydrogen bonds for the first four glucose units of the peeling strand of Figure 14.

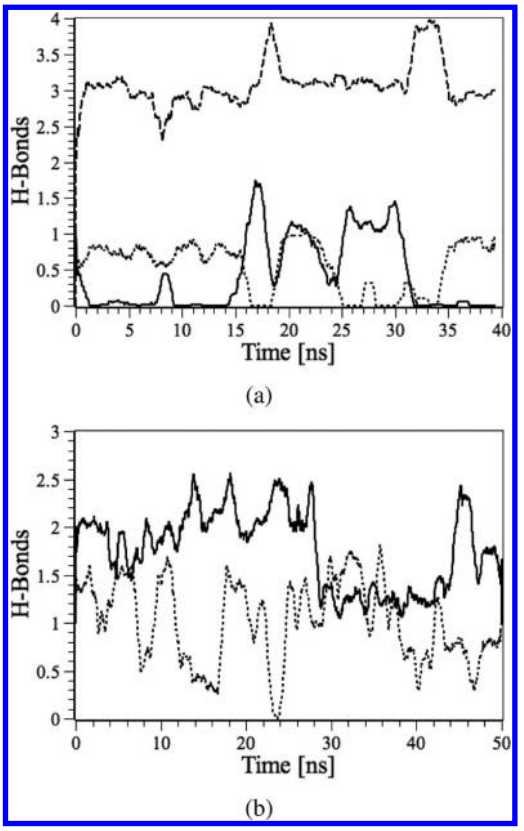

Figure 20. Evolution of hydrogen bonds for (a) the first unit in the nonpeeling, mirror-image strand of Figure 14 and (b) for the first unit of the equivalent strand in SPC/E water. Lines indicate intrastrand (dotted), interstrand (solid), and solvent−strand (dashed) hydrogen bonds.

detached, no peeling is observed for this strand. With the intrastrand hydrogen bonds, and hence the rigidity, still intact there is little chance that this first unit moves away from the main bundle. As soon as the intrastrand hydrogen bonds break, the interstrand hydrogen bonds reattach. This on−off interplay continues for much of the remainder of the simulation, indicating that the breakage of these intrastrand hydrogen bonds could be an integral part of strand peeling.

In water, the hydrogen-bond dynamics of the peeling strand equivalent are shown in Figure 20b. Not only do intrastrand hydrogen bonds never break for a sustained time period, but the interstrand hydrogen bonds remain strong at all times.

dx.doi.org/10.1021/jp310225t | J. Phys. Chem. B 2013, 117, 3469−3479

Together, these analyses suggest that both intrastrand and interstrand breakage might be necessary precursors to the initiation of strand peeling.

CONCLUSIONS

The behaviors of small crystalline bundles of cellulose were examined in both water and three different ILs. The bundle structures were shown to remain intact in water. This stability was quantified by analyzing the evolution of the interstrand hydrogen bonds, showing a stabilization toward a finite number of hydrogen bonds. In the ILs, breakup of strands from the main bundle was observed, and found to follow a single common mechanism for detachment. Anions bind to the hydroxyl groups of cellulose, forming negatively charged moieties. Cations then associate with these attached anions wedging themselves between cellulose strands. In doing so, the bulky size of the cations push these negatively charged moieties apart, leading to strand separation.

These simulations suggest that the individual cations might play a significant role in the initial breakup of cellulose strands during dissolution. Though the arrangement of cation and anion around the cellulose will ultimately determine the IL's ability to dissolve cellulose, this initial breakup could present a substantial barrier for dissolution. The ability of the cation to slip between neighboring strands could be a crucial aspect of an IL's ability to dissolve cellulose and might partially explain why aromatic cations are so effective.

Peeling of an individual strand of cellulose from the Iβ bundles was observed for [EMIM]Ac. This peeling occurred in sudden, disjointed detachments of individual glucose units from the main bundle. By comparing the dynamics of this peeling strand with nonpeeling strands it was observed that the detachment of intrastrand hydrogen bonds for a sustained period as interstrand hydrogen bonds break seems to facilitate strand peeling. Physically, the removal of intrastrand hydrogen bonds broke the structural rigidity of the individual glucose unit allowing it to separate from the main bundle once the interstrand hydrogen bonds were broken as well.

Caution must certainly be exercised when applying the results of models to the actual nature of processes. Other, more detailed phenomena, such as polarizability and charge transfer, were not included due to practical considerations and it still remains to be seen to what degree these considerations might affect behavior. Even so, these results bring attention to some different aspects of cellulose dissolution. It is hoped that these insights might lead to a deeper understanding of the mechanisms by which ILs dissolve cellulose.

ASSOCIATED CONTENT

Supporting Information

Further details including cylindrical distribution functions, detailed breakdowns and evolutions of hydrogen bondiing, and interstrand binding are available. This material is available free of charge via the Internet at http://pubs.acs.org.

AUTHOR INFORMATION

Corresponding Author

*E-mail: brooks.rabideau@avt.rwth-aachen.de; ahmed.ismail@avt.rwth-aachen.de.

Notes

The authors declare no competing financial interest.

ACKNOWLEDGMENTS

Thanks to Jörn Viell for many helpful discussions and ideas for the analysis, Kai Leonhard for a critical reading of the manuscript, and César Ojeda for the use of his script to calculate center-to-center distances between glucan units. This work was performed as part of the Cluster of Excellence "Tailor-Made Fuels from Biomass", which is funded by the Excellence Initiative by the German federal and state governments to promote science and research at German universities.

REFERENCES

(1) Marquardt, W.; Harwardt, A.; Hechinger, M.; Kraemer, K.; Viell, J.; Voll, A. The Biorenewables Opportunity - Toward Next Generation Process and Product Systems. *AIChE J.* **2010**, *56*, 2228−2235.

(2) Swatloski, R.; Spear, S.; Holbrey, J.; Rogers, R. Dissolution of Cellose with Ionic Liquids. *J. Am. Chem. Soc.* **2002**, *124*, 4974−4975.

(3) Sun, N.; Rahman, M.; Qin, Y.; Maxim, M. L.; Rodriguez, H.; Rogers, R. D. Complete Dissolution and Partial Delignification of Wood in the Ionic Liquid 1-Ethyl-3-Methylimidazolium Acetate. *Green Chem.* **2009**, *11*, 646−655.

(4) Vitz, J.; Erdmenger, T.; Haensch, C.; Schubert, U. S. Extended Dissolution Studies of Cellulose in Imidazolium Based Ionic Liquids. *Green Chem.* **2009**, *11*, 417−424.

(5) Zavrel, M.; Bross, D.; Funke, M.; Buechs, J.; Spieß, A. C. High-Throughput Screening for Ionic Liquids Dissolving (Ligno-)Cellulose. *Bioresour. Technol.* **2009**, *100*, 2580−2587.

(6) Viell, J.; Marquardt, W. Disintegration and Dissolution Kinetics of Wood Chips in Ionic Liquids. *Holzforschung* **2011**, *65*, 519−525.

(7) Wasserscheid, P. Chemistry - Volatile Times for Ionic Liquids. *Nature* **2006**, *439*, 797−797.

(8) Wang, H.; Gurau, G.; Rogers, R. D. Ionic Liquid Processing of Cellulose. *Chem. Soc. Rev.* **2012**, *41*, 1519−1537.

(9) Holbrey, J. D.; Seddon, K. R. Ionic Liquids. *Clean Technologies and Environmental Policy* **1999**, *1*, 223−236.

(10) Kahlen, J.; Masuch, K.; Leonhard, K. Modelling Cellulose Solubilities in Ionic Liquids Using COSMO-RS. *Green Chem.* **2010**, *12*, 2172−2181.

(11) Erdmenger, T.; Haensch, C.; Hoogenboom, R.; Schubert, U. S. Homogeneous Tritylation of Cellulose in 1-Butyl-3-Methylimidazolium Chloride. *Macromol. Biosci.* **2007**, *7*, 440−445.

(12) Padmanabhan, S.; Kim, M.; Blanch, H. W.; Prausnitz, J. M. Solubility and Rate of Dissolution for Miscanthus in Hydrophilic Ionic Liquids. *Fluid Phase Equilib.* **2011**, *309*, 89−96.

(13) Zhang, J.; Zhang, H.; Wu, J.; Zhang, J.; He, J.; Xiang, J. NMR Spectroscopic Studies of Cellobiose Solvation in EmimAc Aimed to Understand the Dissolution Mechanism of Cellulose in Ionic Liquids. *Phys. Chem. Chem. Phys.* **2010**, *12*, 1941−1941.

(14) Zhang, J.; Zhang, H.; Wu, J.; Zhang, J.; He, J.; Xiang, J. Reply to "Comment on 'NMR Spectroscopic Studies of Cellobiose Solvation in EmimAc Aimed to Understand the Dissolution Mechanism of Cellulose in Ionic Liquids'" by R. C. Remsing, I. D. Petrik, Z. Liu and G. Moyna, Phys. Chem. Chem. Phys., 2010, 12, DOI: 10.1039/c004203j. *Phys. Chem. Chem. Phys.* **2010**, *12*, 14829−14830.

(15) Remsing, R.; Swatloski, R.; Rogers, R.; Moyna, G. Mechanism of Cellulose Dissolution in the Ionic Liquid 1-n-Butyl-3-Methylimidazolium Chloride: a 13C and 35/37Cl NMR Relaxation Study on Model Systems. *Chem. Commun.* **2006**, 1271−1273.

(16) Remsing, R. C.; Petrik, I. D.; Liu, Z.; Moyna, G. Comment on "NMR Spectroscopic Studies of Cellobiose Solvation in EmimAc Aimed to Understand the Dissolution Mechanism of Cellulose in Ionic Liquids" by J. Zhang, H. Zhang, J. Wu, J. Zhang, J. He and J. Xiang, Phys. Chem. Chem. Phys., 2010, 12, 1941. *Phys. Chem. Chem. Phys.* **2010**, *12*, 14827−14828.

(17) Youngs, T. G. A.; Hardacre, C.; Holbrey, J. D. Glucose Solvation by the Ionic Liquid 1,3-Dimethylimidazolium Chloride: A Simulation Study. *J. Phys. Chem. B* **2007**, *111*, 13765−13774.

(18) Liu, H.; Sale, K. L.; Holmes, B. M.; Simmons, B. A.; Singh, S. Understanding the Interactions of Cellulose with Ionic Liquids: A Molecular Dynamics Study. *J. Phys. Chem. B* **2010**, *114*, 4293−4301.
(19) Liu, H.; Cheng, G.; Kent, M.; Stavila, V.; Simmons, B. A.; Sale, K. L.; Singh, S. Simulations Reveal Conformational Changes of Methylhydroxyl Groups during Dissolution of Cellulose I Beta in Ionic Liquid 1-Ethyl-3-Methylimidazolium Acetate. *J. Phys. Chem. B* **2012**, *116*, 8131−8138.
(20) Liu, H.; Sale, K. L.; Simmons, B. A.; Singh, S. Molecular Dynamics Study of Polysaccharides in Binary Solvent Mixtures of an Ionic Liquid and Water. *J. Phys. Chem. B* **2011**, *115*, 10251−10258.
(21) Gross, A. S.; Chu, J.-W. On the Molecular Origins of Biomass Recalcitrance: The Interaction Network and Solvation Structures of Cellulose Microfibrils. *J. Phys. Chem. B* **2010**, *114*, 13333−13341.
(22) Cho, H. M.; Gross, A. S.; Chu, J.-W. Dissecting Force Interactions in Cellulose Deconstruction Reveals the Required Solvent Versatility for Overcoming Biomass Recalcitrance. *J. Am. Chem. Soc.* **2011**, *133*, 14033−14041.
(23) Gross, A. S.; Bell, A. T.; Chu, J.-W. Thermodynamics of Cellulose Solvation in Water and the Ionic Liquid 1-Butyl-3-Methylimidazolim Chloride. *J. Phys. Chem. B* **2011**, *115*, 13433−13440.
(24) Gross, A. S.; Bell, A. T.; Chu, J.-W. Entropy of Cellulose Dissolution in Water and in the Ionic Liquid 1-Butyl-3-Methylimidazolium Chloride. *Phys. Chem. Chem. Phys.* **2012**, *14*, 8425−8430.
(25) Beckham, G. T.; Matthews, J. F.; Peters, B.; Bomble, Y. J.; Himmel, M. E.; Crowley, M. F. Molecular-Level Origins of Biomass Recalcitrance: Decrystallization Free Energies for Four Common Cellulose Polymorphs. *J. Phys. Chem. B* **2011**, *115*, 4118−4127.
(26) Payne, C. M.; Himmel, M. E.; Crowley, M. F.; Beckham, G. T. Decrystallization of Oligosaccharides from the Cellulose I beta Surface with Molecular Simulation. *J. Phys. Chem. Lett.* **2011**, *2*, 1546−1550.
(27) Jorgensen, W.; Maxwell, D.; TiradoRives, J. Development and Testing of the OPLS All-Atom Force Field on Conformational Energetics and Properties of Organic Liquids. *J. Am. Chem. Soc.* **1996**, *118*, 11225−11236.
(28) Banks, J. Integrated Modeling Program, Applied Chemical Theory (IMPACT). *J. Comput. Chem.* **2005**, *26*, 1752−1780.
(29) Nishiyama, Y.; Sugiyama, J.; Chanzy, H.; Langan, P. Crystal Structure and Hydrogen Bonding System in Cellulose 1(alpha), from Synchrotron X-Ray and Neutron Fiber Diffraction. *J. Am. Chem. Soc.* **2003**, *125*, 14300−14306.
(30) Nishiyama, Y.; Langan, P.; Chanzy, H. Crystal Structure and Hydrogen-Bonding System in Cellulose 1 Beta from Synchrotron X-Ray and Neutron Fiber Diffraction. *J. Am. Chem. Soc.* **2002**, *124*, 9074−9082.
(31) Lopes, J. N. C.; Deschamps, J.; Padua, A. A. H. Modeling Ionic Liquids Using a Systematic All-Atom Force Field (vol 104B, pg 2038, 2004). *J. Phys. Chem. B* **2004**, *108*, 11250−11250.
(32) Ryckaert, J.-P.; Ciccotti, G.; Berendsen, H. J. C. Numerical Integration of the Cartesian Equations of Motion of a System with Constraints: Molecular Dynamics of n-Alkanes. *J. Comp. Phys.* **1977**, *23*, 327−341.
(33) Berendsen, H.; Grigera, J.; Straatsma, T. The Missing Term in Effective Pair Potentials. *J. Phys. Chem.* **1987**, *91*, 6269−6271.
(34) Plimpton, S. J. Fast Parallel Algorithms for Short-Range Molecular-Dynamics. *J. Comput. Phys.* **1995**, *117*, 1−19.
(35) Fernandes, A. N.; Thomas, L. H.; Altaner, C. M.; Callow, P.; Forsyth, V. T.; Apperley, D. C.; Kennedy, C. J.; Jarvis, M. C. Nanostructure of Cellulose Microfibrils in Spruce Wood. *Proc. Natl. Acad. Sci. U. S. A.* **2011**, *108*, E1195−E1203.
(36) Martinez, L.; Andrade, R.; Birgin, E. G.; Martinez, J. M. PACKMOL: A Package for Building Initial Configurations for Molecular Dynamics Simulations. *J. Comput. Chem.* **2009**, *30*, 2157−2164.
(37) Hockney, R. W.; Eastwood, J. W. *Computer Simulation Using Particles*; Adam Hilger-IOP: Bristol, U. K., 1988.
(38) Andersen, H. C. Molecular Dynamics Simulations at Constant Pressure and/or Temperature. *J. Chem. Phys.* **1980**, *72*, 2384.
(39) Rabideau, B. D.; Ismail, A. E. The Effects of Chloride Binding on the Behavior of Cellulose-Derived Solutes in the Ionic Liquid 1-Butyl-3-methylimidazolium Chloride. *J. Phys. Chem. B* **2012**, *116*, 9732−9743.
(40) Chowdhuri, S.; Chandra, A. Hydrogen Bonds in Aqueous Electrolyte Solutions: Statistics and Dynamics Based on Both Geometric and Energetic Criteria. *Phys. Rev. E* **2002**, *66*, 041203.
(41) Chandra, A. Effects of Ion Atmosphere on Hydrogen-Bond Dynamics in Aqueous Electrolyte Solutions. *Phys. Rev. Lett.* **2000**, *85*, 768−771.
(42) Luzar, A.; Chandler, D. Effect of Environment on Hydrogen Bond Dynamics in Liquid Water. *Phys. Rev. Lett.* **1996**, *76*, 928−931.
(43) Luzar, A. Resolving the Hydrogen Bond Dynamics Conundrum. *J. Chem. Phys.* **2000**, *113*, 10663−10675.
(44) Luzar, A.; Chandler, D. Structure and Hydrogen-Bond Dynamics of Water-Dimethyl Sulfoxide Mixtures by Computer-Simulations. *J. Chem. Phys.* **1993**, *98*, 8160−8173.
(45) Luzar, A.; Chandler, D. Hydrogen-Bond Kinetics in Liquid Water. *Nature* **1996**, *379*, 55−57.
(46) Himmel, M. E.; Ding, S.-Y.; Johnson, D. K.; Adney, W. S.; Nimlos, M. R.; Brady, J. W.; Foust, T. D. Biomass Recalcitrance: Engineering Plants and Enzymes for Biofuels Production. *Science* **2007**, *315*, 804−807.
(47) Matthews, J. F.; Beckham, G. T.; Bergenstrahle-Wohlert, M.; Brady, J. W.; Himmel, M. E.; Crowley, M. F. Comparison of Cellulose I Beta Simulations with Three Carbohydrate Force Fields. *J. Chem. Theory Comput.* **2012**, *8*, 735−748.
(48) Paavilainen, S.; Róg, T.; Vattulainen, I. Analysis of Twisting of Cellulose Nanofibrils in Atomistic Molecular Dynamics Simulations. *J. Phys. Chem. B* **2011**, *115*, 3747−3755.
(49) Kirschner, K. N.; Yongye, A. B.; Tschampel, S. M.; González-Outeiriño, J.; Daniels, C. R.; Foley, B. L.; Woods, R. J. GLYCAM06: a Generalizable Biomolecular Force Field. Carbohydrates. *J. Comput. Chem.* **2008**, *29*, 622−655.